Vasyukova, O. V., Williams-Jones, A.E., 2019. Tracing the evolution of a fertile REE granite by modelling amphibole-melt partitioning, the Strange Lake story. Chemical Geology, 514: 79-89.

Tracing the evolution of a fertile REE granite by modelling amphibole-melt partitioning, the Strange Lake story

O.V. Vasyukova and A.E. Williams-Jones

Department of Earth and Planetary Sciences, McGill University, 3450 University Street, Montreal, Québec, Canada, H3A 0E8, olga.vasyukova@mcgill.ca

Abstract

In principle, potentially economic (fertile) granites can be distinguished from uneconomic (barren) granites based on the composition of their magmas. Ideally, this composition would be evaluated by analysing melt inclusions, but such inclusions are rarely preserved and difficult to analyse. Information on the composition of magmas can also be obtained from the composition of the minerals crystallising from these magmas, if the mineral-melt partition coefficients are known. In some cases where these partition coefficients are not known, they have been calculated from lattice strain theory. Here we report arfvedsonite-melt partition coefficients for the rare earth elements (REE) calculated from the results of analyses of arfvedsonite, bulk rock and melt inclusions in granites and pegmatites in the Strange Lake peralkaline rare metal pluton. These coefficients were fitted to the lattice strain model from which values of the ideal partition coefficient (D_0), the ideal radius (r_0) and the elastic response (E_M) were determined. The light REE were shown to partition preferentially into the M4 site and the HREE into the M2 site, requiring that partition coefficients be calculated for each site. The partition coefficients for both sites were shown to decrease systematically with increasing evolution of the magma, i.e., from the early hypersolvus granite to the late pegmatites. In the case of the M4 site, D_0, r_0 and E_M vary linearly with the Ca content of the arfvedsonite. By contrast, these parameters for the M2 site vary linearly with temperature. The two relationships form the basis of a predictive model in which the arfvedsonite-melt REE partition coefficients for any peralkaline granite can be estimated, provided that the Ca content of the amphibole and its crystallisation temperature are known. This model was applied to a peralkaline granitic pegmatite from the Amis complex (Namibia) for which data on the composition of the amphibole and corresponding magma (melt inclusions) have been reported. The model successfully predicts the concentrations of the various REE in this magma, thereby providing confidence that it can be used to discriminate between granites that are potentially fertile and those that are barren in respect to the REE.

Keywords: Peralkaline granites and pegmatites; Rare Earth Elements; Arfvedsonite; Mineral-melt partition coefficients; Lattice strain model

Introduction

To investigate the genesis of magmatic-hydrothermal deposits, it is necessary to start by considering the processes that concentrate metals in the magmas. In principle, much of the necessary information for such investigations can be obtained from analyses of melt inclusions. For many magmatic-hydrothermal systems, however, melt inclusions are either not preserved or are difficult to analyse reliably. In contrast, the minerals crystallising in these systems preserve a record in their trace element chemistry that reflects the concentration of the metals of interest in the coexisting magma. If the mineral-melt partition coefficients for these metals are known, their concentrations in the mineral will allow the corresponding metal concentrations in the coexisting magma to be estimated.

Many studies have investigated the partitioning of metals between minerals and melts (e.g., Wood and Blundy, 1997; Bottazzi et al., 1999; Blundy and Wood, 2003; Olin and Wolff, 2010; Wood and Blundy, 2014), particularly for the rare earth elements (REE), because of their importance in modeling magmatic processes. There is also a widely employed model for determining mineral-melt partitioning, namely, the lattice strain model (Blundy and Wood, 2003). However, accurate determination of magma composition using this model remains a challenge. The reason for this is that it is difficult to reliably estimate the values of the main parameters in the lattice strain equation (D_0, r_0 and E_M), because of their dependence on a variety of factors including the structure and composition of the mineral.

In this paper, we report results for the partitioning of the REE (La to Lu) between amphibole and melt in a peralkaline granitic pluton (Strange Lake) that hosts potentially economic concentrations of the REE, and use these data to reconstruct the path taken by the REE during successive stages of magma emplacement. Based on this reconstruction we develop a model using lattice strain theory that successfully predicts the evolving REE distribution in the Strange Lake magma and is applicable to other peralkaline granitic intrusions for which melt inclusion data are not available. It is hoped that the insights gained from this study will prove helpful in understanding the magmatic processes that concentrate the REE in peralkaline igneous systems.

Geological setting

The Strange Lake pluton, which is Mid-Proterozoic in age (1240 ± 2 Ma, Miller et al., 1997), comprises three main intrusive phases, namely hypersolvus granite (a single alkali feldspar), transsolvus granite (three alkali feldspars) and pegmatite (Fig. 1). The earliest and the least evolved phase is the hypersolvus granite, which occupies the central part of the intrusion, and is characterised by the presence of perthite as the only feldspar and interstitial arfvedsonite. This phase is subdivided into two sub-phases, namely, a primitive southern hypersolvus granite and a more evolved northern hypersolvus granite. Both are locally accompanied by pegmatitic segregations. Perthite is also present in the transsolvus granite, which is more evolved than the hypersolvus granites, volumetrically much more abundant, and occupies the outer part of the pluton. In addition, however, the transsolvus granite contains primary microcline and albite, and the arfvedsonite, instead of being an interstitial phase, occurs as phenocrysts.

The three granite types discussed above also contain a variety of rare-earth element (REE), Nb, Zr and Ti minerals and fluorite (Table 1). In the hypersolvus granites, the primary REE-bearing minerals are monazite-(Ce) and pyrochlore-group minerals, which generally occur as euhedra and are, therefore, interpreted to have crystallised early. Zirconium also crystallised early, as zircon euhedra, and later, as the alkali zirconosilicate minerals, vlasovite and dalyite, which commonly contain relicts of primary zircon. There are no primary Ti minerals. Fluorite is common, particularly as blebs, interpreted by Vasyukova and Williams-Jones (2014, 2016) to represent an immiscible fluoride melt. The primary REE minerals in the transsolvus granite include early monazite-(Ce) and pyrochlore but also later crystallising gagarinite-(Ce) that occurs almost invariably in association with arfvedsonite. In contrast to the hypersolvus granites, there is no primary zircon in the transsolvus granite. Instead, the primary Zr mineral is vlasovite, which commonly contains numerous inclusions of microcline and albite creating a poikilitic texture. The primary Ti mineral is narsarsukite. Fluorite is commonly observed either as bleb-like inclusions in arfvedsonite or as amoeboid masses attached to gagarinite-(Ce). As in hypersolvus granites, the fluorite is interpreted to crystallised from a fluoride melt (Vasyukova and Williams-Jones, 2014; Vasyukova and Williams-Jones, 2016).

The pegmatites, which host the bulk of the potentially economic REE mineralisation, occur near the top of the pluton as sub-horizontal sheets and lenses within transsolvus granite, and range from a few cm to 10 m in thickness. They are concentrated in two fields, one adjacent to the northwest margin of the pluton, the B-Zone, and the other near its geographic centre, the Main-

Zone (Fig. 1). The REE mineralisation is accompanied by significant Zr and Nb mineralisation for an indicated resource of 278 Mt of ore, grading 0.94 wt. % REE_2O_3 (38% heavy rare-earth oxides), 1.92 wt. % ZrO_2 and 0.18 wt. % Nb_2O_5 (www.questrareminerals.com). Many of the pegmatites are mineralogically zoned from a border containing coarse-grained euhedral alkali feldspar, quartz, arfvedsonite and titano- and zircono-silicate minerals to a core dominated by quartz and fluorite with variable proportions of REE minerals; the only other primary HFSE minerals are elpidite and narsarsukite. The contacts between the pegmatites and the transsolvus granite are gradational.

Evidence of hydrothermal alteration is widespread in the transsolvus granite, and increases in intensity towards the pegmatite fields. Perthite and K-feldspar in the transsolvus granite were albitised, and arfvedsonite was altered to aegirine ± hematite. Calcium metasomatism was pervasive in the pegmatites and locally pervasive in the adjacent transsolvus granite, leading to the replacement of sodium titanosilicates and zirconosilicates by calcium minerals such as titanite and gittinsite ($CaSi_2O_7$), respectively. Finally, late phyllic alteration, manifested by the replacement of primary and secondary feldspars by Al-phyllosilicates and arfvedsonite by Fe-rich phyllosilicates, was also pervasive in the pegmatites and developed locally in the adjacent transsolvus granite. For further information on the geology and mineralogy of the Strange Lake pluton, readers are referred to the papers of (Salvi and Williams-Jones, 1995; 1996; Gysi and Williams-Jones, 2013; Vasyukova and Williams-Jones, 2014; Gysi et al., 2016; Vasyukova and Williams-Jones, 2016; Siegel et al., 2017; Siegel et al., 2018).

Methodology

The study presented here is based on bulk rock compositions for the hypersolvus and transsolvus granites reported in Siegel (2018), arfvedsonite compositions from the hypersolvus and transsolvus granites in Siegel (2018) and melt inclusion and arfvedsonite compositions from pegmatites analysed (this study). The melt inclusions (they were homogenised by heating to 700 ^{o}C at 3 kbar and quenched) and arfvedsonite were analysed using a combination of electron microprobe (EMP) and laser ablation induced coupled plasma mass spectrometry (LA-ICP-MS) methods.

The EMP analyses were carried out with a JEOL JXA-8900L electron microprobe at McGill University (Department of Earth and Planetary Sciences), using a beam diameter of 15 μm, a beam current of 20 nA and an acceleration voltage of 20 kV for arfvedsonite. A beam diameter

of 15-20 μm, a beam current of 6.5 nA and an acceleration voltage of 15 kV were used for the melt inclusions.

The LA-ICP-MS analyses of arfvedsonite were carried out on the same spots analysed using the EMP, and were carried out using a NewWave 213 nm Nd-YAG laser-ablation system and a Thermo Finnigan iCapQ ICP-MS in the Department of Earth and Planetary Sciences at McGill University. The method involved a 10 Hz repetition rate, and 40 μm beam diameter; the NIST 610 glass was used as an internal standard for Si. The LA-ICP-MS analyses of the melt inclusions were conducted in traverse mode on a Thermo X Series II inductively coupled quadrupole mass spectrometer at the Great Lakes Institute for Environmental Research (GLIER), University of Windsor. The analyses involved an energy of approximately 5 mJ, a repetition rate of 5 Hz and a spot size of 35 μm. Data from the EMP analyses were used to normalise the LA-ICP-MS data. The results of these analyses and those of Siegel (2018) are reported in Tables 2 and 3.

Results

Data treatment

Arfvedsonite-melt partition coefficients for the different granite facies (Fig. 2) were calculated from the REE contents of arfvedsonite and the bulk REE content of the corresponding granite on the assumption that the latter represents the REE content of the melt. As we were able to find melt inclusions in the pegmatites (border zone, Figs. 2a and b) and measure their compositions, we used these data to calculate the partition coefficients for this facies. The compositions of the arfvedsonite used in the calculations are reported in Table 2 and their chondrite-normalised REE profiles are shown in Figure 3a. In order to reliably determine arfvedsonite-melt partition coefficients using bulk rock compositions, it is essential that the latter correspond to the melt composition at the time of crystallisation of the arfvedsonite. We, therefore, corrected the bulk rock REE content to account for prior crystallisation of feldspar and for the small proportion of fluoride magma (this melt contains ~25 wt. % REE) that exsolved from the silicate melt (Vasyukova and Williams-Jones, 2014; Vasyukova and Williams-Jones, 2016). In the case of the transsolvus granite (Fig. 2c and d), we also corrected for the fact that the magma crystallising the pegmatites was a residue of the transsolvus granite magma; this is evident from the gradational contact between transsolvus granite and pegmatite (Fig. 2a). No correction was applied to the melt inclusion composition as it represents the composition of the magma from which the arfvedsonite crystallised.

In the case of the hypersolvus granites, arfvedsonite is interstitial to the feldspar (perthite) and arfvedsonite clearly crystallised later than the feldspar (Figs. 2e and f). As perthite is the only mineral containing concentrations of Al above ppm levels, we can assume that all of the Al is contained in this mineral. We calculated the mass proportion of the perthite from the ratio of the Al_2O_3 content of the rock to that of the perthite. This proportion was removed from the bulk rock composition and the latter normalised to 100 %. In the transsolvus granite, all the perthite and part of the later crystallising albite and microcline formed before arfvedsonite, as shown by the fact that albite and microcline are present as inclusions in arfvedsonite (Fig. 2d). Based on petrographic observations, we estimate that ~ 30 % of the feldspar crystallised before arfvedsonite. This feldspar was removed, and the residual rock composition was normalised to 100 %.

The proportion of fluoride melt that exsolved from the magmas, which crystallised the different granite types, was estimated by relating the Ce content of this melt reported in Vasyukova and Williams-Jones (2016) to the bulk rock Ce content. As the silicate fraction of the magma contained an appreciable concentration of Ce, the estimation also involved correcting for this contribution. We used Ce in our calculations because the fluoride melt is dominated by the light REE (LREE), and Ce is the principal LREE. Inasmuch as the northern hypersolvus granite is the least evolved granite for which we have evidence of a fluoride melt and the southern hypersolvus granite is less evolved, we assumed for the purpose of our calculations that the southern hypersolvus granite did not exsolve a fluoride melt and that the REE content of the silicate fraction of the northern hypersolvus granite was the same as the REE content of the southern hypersolvus granite. The proportion of fluoride melt in the northern hypersolvus granite was accordingly estimated to be 0.2 wt. %. We have no means of reliably estimating the relative proportions of silicate and fluoride melt in the transsolvus granite. If, however, we assume that they were the same as for the northern hypersolvus granite, then the transsolvus granite would have contained 0.75 wt. % fluoride melt.

We removed 0.2 wt. % of the fluoride melt from the bulk composition of the northern hypersolvus granite and normalised the remainder to 100 %. In the case of the transsolvus granite, we removed 0.75 wt. % of the fluoride melt and added back a proportion of the pegmatite melt (40 wt.%). The latter was done because the pegmatites are considered to have crystallised from residues of the transsolvus granite magma, and the proportion is high because the transsolvus granite was sampled close to pegmatite (see above).

The effects of the various corrections described above are illustrated in Figures 3b and c, which show the chondrite-normalised distribution of the REE in the different granites and pegmatite before and after correction, respectively. From this figure it is evident that a major effect of the corrections was to decrease the difference in the concentrations of the REE in the hypersolvus granites from those of the transsolvus granite and pegmatite. The other important effect was to bring the profile of the transsolvus granite into parallelism with those of the other facies. This was due largely to the restoration of the residual melt that separated from the transsolvus granite to form the pegmatites. The initial and corrected bulk REE contents of the granites referred to above are reported in Tables 3 and 4, the REE content of the pegmatite melt inclusions in Table 3 and the arfvedsonite-melt partition coefficients in Table 5.

Arfvedsonite-melt partition coefficients

The REE partition coefficients are highest for the southern hypersolvus granite and decrease progressively through the northern hypersolvus granite and the transsolvus granite to the pegmatite (Table 5). As the ability of a mineral to incorporate trace elements depends to a large extent on the size of the corresponding ions relative to that of the site into which they are incorporated, partition coefficients are commonly illustrated in diagrams showing their distribution as a function of ionic radius (Onuma diagrams, Blundy and Wood, 2003). This distribution defines a parabola with a maximum corresponding to the ideal radius of the site. In the case of the alkali amphiboles minerals, there are two sites into which the REE are known to partition, namely the 6-fold M2 site and the larger 8-fold M4 site (Bottazzi et al., 1999). The light REE (LREE), having larger ionic radii than the heavy REE (HREE), will tend to concentrate in the M4 site, whereas the HREE will concentrate in the M2 site (Bottazzi et al., 1999). With this in mind, we plotted the arfvedsonite-melt partition coefficients for the different granite types and pegmatite in Figure 4a as a function of ionic radius. Their distribution can be described by a complete parabola from La to Gd for the M4 site and a partial parabola (high ionic radius limb) for Tb to Lu for the M2 site. In order to complete the parabola for the M2 site, we added Sc, which has an ionic radius of 0.75, to our list of REE. Unfortunately, we only have reliable data for the northern hypersolvus granite and the pegmatite as the concentration of Sc in the bulk rock of the other granite facies was below the limit of detection. In the southern hypersolvus granite, the arfvedsonite-melt partition coefficient for the M4 site reaches a maximum of 0.96 at a radius corresponding to that of Sm (1.08 Å). The maximum decreases progressively through the northern hypersolvus granite (0.18) and the transsolvus granite (0.012) to the pegmatite (0.003). The ionic radius of the maximum increases progressively to that of Nd (1.109) for the transsolvus granite and the pegmatite. For comparison, in Figure 4a, we show the

ideal ionic radii for the M4 site (1.12 Å) for an alkali amphibole modelled by Bottazzi et al. (1999); their ideal radius for the M2 site (also shown) is 0.72 Å. The highest partition coefficient for the M2 site is that of Lu, which increases progressively by over one order of magnitude from a value of 0.14 for the pegmatite to 3.0 for the southern hypersolvus granite. There is also a progressive increase in the slope of the distribution of the partition coefficients for the pegmatite to that of the southern hypersolvus granite (Fig. 4a).

Discussion

Modelling mineral-melt partitioning

In the preceding section, we showed that the arfvedsonite-melt partition coefficients for the REE are controlled to a large extent by the properties of the sites, which accommodate these elements in arfvedsonite. We also showed that the HREE partition preferentially into the six-fold co-ordinated M2 site and the LREE into the eight-fold co-ordinated M4 site.

The above behaviour can be explained by the lattice strain model, which depends on temperature, the elasticity of the crystal lattice and the ideal radius of the site into which the element partitions (Blundy and Wood, 2003). According to this model, the partition coefficients for a suite of elements of the same charge will reach a maximum for the cation that has an ionic radius closest to the ideal ionic radius for the site in question, and will decrease progressively with increasing and decreasing ionic radius of the elements, producing a parabolic distribution. The rate at which the partition coefficient decreases with ionic radius away from the ideal radius is determined by the elasticity of the lattice, and thus the distribution of partition coefficients for an elastic lattice will be described by a relatively broad parabola, whereas a rigid lattice will produce a narrow parabolic distribution. This qualitative description is formalised in the lattice strain model by the equation:

$$D_i = D_0 \exp\left\{\frac{-4\pi E_M N_A}{RT}\cdot\left[\frac{r_0\left(r_i - r_0\right)^2}{2} + \frac{\left(r_i - r_0\right)^3}{3}\right]\right\} \quad (1)$$

which relates the equilibrium partition coefficient D_i for a cation with radius r_i entering a crystal lattice site, M. In this equation, D_0 is the partition coefficient of an isovalent cation of radius r_0, which enters the site without strain, E_M is the Young's modulus of site M, N_A is Avogadro's Number, R is the universal gas constant, and T is temperature in Kelvin (Blundy and Wood,

2003). The value for D_0 for a cation with the ideal radius, r_0, establishes the 'height' (maximum) of the parabola, the curvature of which is controlled by T and E for the site M. Thus, the parameters, D_0, r_0, E_M and T determine the partition coefficients D_i for the elements of interest (in our case the REE) having a radius r_i.

We modelled the data presented in Table 5 and Figure 4a for the two sites (M2 and M4) by fitting them to equation (1), and solving for the parameters D_0, r_0 and E_M for each site. In order to do this, it was necessary to assign crystallisation temperatures for arfvedsonite in each of the granite facies and the pegmatite. The only units for which we have reliable estimates of these temperatures are the northern hypersolvus granite and the pegmatite. The temperature for the former was estimated by Siegel et al. (2018) to be 660 ^{o}C based on oxygen isotope fractionation for the pair arfvedsonite-quartz. The minimum temperature for the crystallisation of the pegmatite was estimated to be 425 ^{o}C based on homogenisation temperatures of fluid inclusions coexisting with melt inclusions (Vasyukova et al., 2016). A somewhat higher temperature of 450-500 ^{o}C was proposed by Vasyukova et al. (2016) for the emplacement of pegmatite magma. For the purpose of our modelling, we assumed that the arfvedsonite crystallised at 450 ^{o}C. As the southern hypersolvus granite magma was less evolved and crystallised earlier than the northern hypersolvus granite magma, arfvedsonite was assumed to have crystallised at slightly higher temperature than in the latter, i.e., 675 ^{o}C. The temperature for the transsolvus granite is more difficult to constrain. The observation, however, that the pegmatites crystallised from residual transsolvus granite magma suggests that the temperature of crystallisation of arfvedsonite in the transsolvus granite magma was lower than that of the hypersolvus granites. We have assumed a temperature of 600 ^{o}C.

The results of this modelling are illustrated in Figure 4b. In the case of the M2 site, it can be seen that, with increasing ionic radius of the REE, the calculated D_i values deviate systematically to values lower than those measured. This effect is most marked for the southern hypersolvus granite. We believe that the most plausible explanation for the deviations of the calculated D_i for the REE in the M2 site is that significant proportions of the MREE (Tb to Ho) entered both the M2 and M4 sites. This is because these REE have ionic radii intermediate between those of the ideal radii of the M4 and M2 sites. We, therefore, corrected the calculated D_i for each REE by summing the contributions modelled for the two sites. The MREE with the lowest D_i was identified and all REE with higher D_i and lower ionic radii were assigned to the M2 site. The remaining REE were assigned to the M4 site. In Figure 4c, we illustrate the corrected distribution

of the arfvedsonite-melt REE partition coefficients for the different granitic facies and pegmatite. The corresponding values of D_0, r_0 and E_M are reported in Table 6.

Partitioning parameters for the M4 site (r_0, E_M and D_0)

As noted earlier, the ideal radius (r_0) for the M4 site reported by Bottazzi et al. (1999) for K-richterite is 1.12 Å. This radius is the same as the ionic radius of Ca, an observation that Bottazzi et al. (1999) used to conclude that the LREE are incorporated selectively in M4 sites occupied by Ca. From Table 6 and Figure 4, it is evident that the ideal radii modelled in the current study are similar to, albeit a little smaller than that interpreted by Bottazzi et al. (1999), supporting a conclusion that the LREE partition preferentially into M4 sites that otherwise would be occupied by Ca (1.12 Å). We propose that the M4 sites for Ca were made available by the substitution of Al^{3+} for Si^{4+} in the tetrahedral site. This would have increased the size of the tetrahedral site significantly, and also increased the negative charge on the tetrahedra. Consequently, the size of the adjacent M4 site would have decreased in response to the resulting decrease in the bond length and increase in the bond strength. This interpretation is supported by the observation that the arfvedsonite content of Al, which is entirely in the tetrahedral site, shows an excellent positive correlation with the Ca content (Fig. 5a). It should, therefore, follow that the above substitution (Al^{3+} for Si^{4+}) would also have facilitated the incorporation of the LREE in the M4 site, as the LREE are closer in size to Ca than they are to Na. This explanation is consistent with the observation that the LREE concentrations show an excellent positive linear correlation with Al concentration in the arfvedsonite (Fig. 5b). A final test of the hypothesis developed above are the relationships of r_0 with Ca and Al. The hypothesis predicts that the number of M4 sites available for Ca and LREE should increase with the concentration of Al and this should be reflected in linear inverse correlations of r_0 with Ca (Fig. 6a) and with Al. This is the case for the two hypersolvus granites and the transsolvus granite; the correlation is nearly perfect. The r_0 value for the pegmatite, however, plots below the trend for the granites (Fig. 6a). We propose that the reason for this is that the pegmatite magma exsolved a fluid with a relatively high content of the LREE (Vasyukova and Williams-Jones, 2018). As a result, the melt no longer reflects the evolution of the Strange Lake magmas as it was depleted in these highly incompatible elements making its composition representative of a less evolved magma. Our subsequent discussion of the lattice strain parameters, therefore, is restricted to the two hypersolvus granites and the transsolvus granite.

Above, we noted that r_0 shows a nearly perfect inverse linear correlation with the Ca content of the arfvedsonite for the two hypersolvus granites and the transsolvus granite. The same is true for E_M (Fig. 6b). We believe that the reason for this is that by adding Ca to the M4 site, the elasticity of the crystal lattice is increased through the creation of a mixture of smaller (Ca) and larger (Na) sites.

In contrast to r_0 and E_M, D_0 increases linearly with increasing Ca content of the arfvedsonite (Fig. 6c). The reason for the increase of D_0 with Ca is that the LREE, as noted earlier, occupy the same M4 sites as Ca and thus the greater availability of Ca will facilitate greater occupancy of LREE in these sites and, in turn, lead to higher arfvedsonite-melt partitioning of the LREE and correspondingly higher D_0 values.

Partitioning parameters for the M2 site (r_0, E_M and D_0)

In contrast to the LREE, our measured partition coefficients for the HREE do not reach a maximum and consequently do not predict a r_0 value for the M2 site. However, our modelling predicts values of r_0 ranging from 0.77 to 0.80 (Table 6 and Fig. 4c). These radii are slightly larger than that of Sc (0.75 Å), which helps define the low ionic radius limb of the parabola for the northern hypersolvus granite and the pegmatite. They are also very close to the ionic radius of Fe^{2+} (0.78), the main cation in the M2 site, indicating that the HREE substituted for this cation. There is a strong positive correlation between r_0 and the temperature of arfvedsonite crystallisation (Fig. 6d), which is consistent with the prediction that the radii of crystal sites increase with increasing temperature due to the corresponding increase in vibrational energy and the weakening of the metal-oxygen bond. Values for E_M decrease linearly with temperature (Fig. 6e). This is because the crystal lattice becomes more elastic at higher temperature. Like r_0, D_0 increases linearly with temperature (Fig. 6f). This correlation can be explained by the corresponding increase in the vibrational energy and resulting weakening of the REE-O bond in the arfvedsonite, allowing the M2 site to accommodate greater concentrations of the REE.

The validity of the model

A comparison of the measured melt compositions with those modelled indicates that, with few exceptions, the modelled REE contents differ by < 25 % from the measured compositions and for most REE this difference is less than 10 % (Fig. 7; Table 7). The exceptions are La in the northern hypersolvus granite and the transsolvus granite for which the difference reaches ~ 300 %, Gd and Tb in the transsolvus granite for which the modelled concentrations are 80 and 68 %

lower than measured, and Eu in the pegmatite, for which it is 28 % less than measured. We attribute the large differences associated with La to problems with the analyses of arfvedsonite, possibly a peak interference, which lead to anomalously high values of D_i; the concentration of La in arfvedsonite is anomalously high as illustrated in Figure 3a (Figure 4a). The relatively large difference between the measured and modelled partition coefficients for Gd and Tb may reflect errors in the measured values (the concentrations of Gd and Tb in the arfvedsonite (1.21 and 0.27 ppm) are the lowest of all of the REE except for that of Eu (0.07 ppm); Table 2). The difference in the case of Eu is almost certainly due to the low measured concentration and the correspondingly high analytical uncertainty. Thus, in summary, the lattice strain model applied with the corrections described above reliably estimates the concentrations of most of the REE in the various granitic facies of the Strange Lake pluton.

An application of the model

In principle, the model that we have developed for Strange Lake should be applicable in predicting REE arfvedsonite-melt partition coefficients for other peralkaline granitic plutons. The only pluton, to our knowledge, for which the REE composition of both the arfvedsonite and the magma (melt inclusions) have been measured is the Amis pluton in Namibia (Schmitt et al., 2002). In the paragraphs below, we discuss the application of our model to this pluton.

As mentioned earlier, the D_0, E_M and r_0 values for the M4 site vary linearly with the Ca content of the arfvedsonite (Figs. 6 a-c, Table 7). We have used these relationships to model the partition coefficients (D_i) for the M4 site in the Amis arfvedsonite. The arfvedsonite from the sample (granitic pegmatite), for which Schmitt et al. (2002) report melt inclusion data, has a CaO content of 0.67 wt. % (Table 8). This is within the range of the CaO contents of the arfvedsonite in the Strange Lake granites considered in this study (1.80 to 0.12 wt.%). The arfvedsonite-melt REE partition coefficients for the M4 site of the Amis sample were, therefore, modelled using D_0, E_M and r_0 values corresponding to those predicted by the linear correlations referred to above (Figs. 6 a-c).

In contrast to the M4 site, the D_0, E_M and r_0 values for the M2 site are independent of the CaO content of the arfvedsonite but vary linearly with the temperature of crystallisation of the arfvedsonite (Figs. 6d-f). We, therefore, modelled the arfvedsonite-melt REE partition coefficients for the M2 site of the Amis sample assuming that the D_0, E_M and r_0 values can be predicted reliably from the temperature of the magma. According to Schmitt et al. (2002) glass channels appeared in their melt inclusions when heated to 600 °C and the inclusions

homogenised completely when the temperature reached 650 °C. For the purpose of our modelling, we have assumed an intermediate temperature for arfvedsonite crystallisation of 620 ^{o}C.

In Figure 8, we show the arfvedsonite-melt REE partition coefficients for the Amis granitic pegmatite calculated from the average compositions of the arfvedsonite and melt inclusions in Schmitt et al. (2002). Also shown on this figure are the modelled partition coefficients (D_i). From this figure, it is evident that the modelled values of D_i are very close to those calculated (measured), except for La and Eu. The values for La and Eu depart strongly from the parabolic distribution of the measured D_i values for the M4 site, indicating that they almost certainly reflect analytical errors. As was the case for the Strange Lake northern hypersolvus and transsolvus granites, the problem with La was likely in the analysis of arfvedsonite (peak interference; see above). For Eu, the problem was likely the fact that the concentration in both the arfvedsonite and the melt inclusions was very low (< 1 ppm, Table 8), approaching that of the detection limit.

The concentrations of the REE in the melt estimated by our model are within 15 % of those measured by Schmitt et al. (2002), except for La, Eu and Yb (Table 9). As expected from our previous comments, the errors for La and Eu are extremely high (235 and 238 %, respectively). The error for Yb is 27 %. Thus, the model developed in this paper predicts the composition of the Amis pegmatite magma remarkably well.

In applying the model to plutons other than Strange Lake and Amis there are several caveats that need to be applied. The first is that the CaO content of the arfvedsonite should be broadly within the range of CaO contents of the Strange Lake arfvedsonite, i.e., between 0.1 and 1.8 wt. %. The second is that the temperature of amphibole crystallisation should be within the range from ~ 450 to ~ 700 ^{o}C. Finally, the magma should not have reached fluid phase separation prior to the crystallisation of the amphibole.

The REE, arfvedsonite and magma evolution

In the preceding sections, we have shown that the arfvedsonite-melt REE partition coefficients for the LREE (M4 site) increase linearly with the Ca content of the amphibole, which, in turn, increases with the Ca content of the magma. In contrast, the arfvedsonite-melt REE partition coefficients for the HREE (M2 site) increase linearly with the temperature of crystallisation of arfvedsonite. These observations should, in principle, allow us to quantitatively predict the role

that arfvedsonite plays in determining the path of REE concentration in an evolving peralkaline granitic magma.

The arfvedsonite-melt REE partition coefficients for the M4 site are all < 1 for the CaO contents of the arfvedsonite considered in this study (up to 1.8 wt. %), indicating that the LREE partition preferentially into the melt (Table 5). Thus, the effect of arfvedsonite crystallisation is to increase the proportion of the LREE in the magma. The arfvedsonite-melt partition coefficients for some of the HREE, however, are greater than unity. In the case of Lu, the partition coefficient reaches 4.6 for the highest temperature considered in our study (675 ^{o}C). This partition coefficient would increase to 5.9, if the temperature were raised to 700 ^{o}C. The corresponding partition coefficients for Yb and Tm would be 4.5 and 3.6, respectively. Thus, in contrast to the LREE, at least at high temperature, some of the HREE favour the amphibole, thereby, depleting the magma in HREE. Nonetheless, it is important to note that at temperatures below 625 ^{o}C, the partition coefficients for all the HREE are <1 and arfvedsonite crystallisation will lead to the enrichment of both LREE and HREE in the magma.

From the above discussion, it is evident that the effect of arfvedsonite crystallisation on the REE composition of the magma depends heavily on temperature and the CaO content. If a peralkaline granitic magma evolves by fractional crystallisation of arfvedsonite and the temperature is greater than 625 ^{o}C, the magma would be progressively depleted in the HREE (Lu would be the first to be depleted, and would be joined by Yb at ~ 650 ^{o}C and Tm at ~ 670 ^{o}C). The LREE, however, would be enriched in the magma at all the temperatures (up to 675 ^{o}C) and CaO contents considered in this study (up to 1.8 wt. %). The effects described above are illustrated in Figure 9, which shows the distribution of melt-arfvedsonite partition coefficients for the different REE as a function of temperature. In Figure 9a, we show the partition coefficients for a magma composition corresponding to that of the northern hypersolvus granite, the arfvedsonite of which has a CaO content of 0.47 wt. %. This figure emphasises the temperature independence of the partitioning of the LREE (M4) and the sensitivity of the partitioning of the HREE to temperature. Figure 9b was constructed to illustrate the combined effects of temperature and CaO content on the arfvedsonite-melt REE partition coefficients, and was based on the data presented earlier for the Strange Lake granites and pegmatite. From this figure it can be seen that at high temperature and high CaO content arfvedsonite crystallisation will lead not only to a depletion in the HREE but also in the MREE starting with Sm and Eu (the melt-mineral partition coefficients for Sm and Eu are unity at 675 and 1.8 wt. % CaO and will decrease with increasing temperature and CaO content). The other important observation is that, irrespective of temperature, in relative

terms, the magma would be preferentially enriched in the MREE (Sm to Dy) and the LREE (La, Ce), whereas, it would be depleted in the heavy REE. Moreover, it can also be seen that this fractionation of the REE increases with decreasing temperature and CaO content, i.e., with the evolution of the magma (Fig. 9b).

Predicting the REE fertility of peralkaline granitic plutons

In principle, it should be possible to apply the model developed above in predicting the degree of fertility of any arfvedsonite-bearing A-type granite and its pegmatites. To do this, all that would be required are data on the CaO and REE content of the arfvedsonite from two or more members of a granite suite that has evolved by fractional crystallisation, and estimates of the temperature of arfvedsonite crystallisation. The latter could be determined from the isotopic fractionation of oxygen between arfvedsonite and quartz. Whether the evolution leads to potentially economic mineralisation depends heavily on the initial temperature and Ca content of the magma. If both are high, i.e., very much greater than 675 ^{o}C and 1.8 wt. % CaO, the REE will prefer the arfvedsonite strongly over the melt (see above), and, consequently, arfvedsonite crystallisation will lead to significant depletion in the REE, particularly the highly sought after HREE. Thus, for a pluton to be fertile, the arfvedsonite of the least evolved granite should have a low CaO content and have crystallised at a temperature significantly less than 675 ^{o}C (Fig. 9). Late crystallisation of arfvedsonite in this granite would also ensure that there was no depletion in the REE due to prior crystallisation of arfvedsonite in the magma chamber. With magma evolution the Ca and REE contents of the arfvedsonite would decrease progressively, signalling the development of a fertile pluton.

The requirements for fertility were met at Strange Lake, a pluton that, as discussed, earlier hosts a potentially economic REE deposit. Thus, as expected, arfvedsonite was a late phase in the earliest granite (southern hypersolvus), and had a relatively low CaO content. It also crystallised at relatively low temperature (675 ^{o}C). Despite this, the crystallisation of arfvedsonite lead to the depletion of the residual magma in several HREE, namely, Er to Lu. Consequently, although there was an overall REE enrichment in the pegmatites crystallising from the residues of this magma (2785 versus 2305 ppm total REE; Table 4), there was a predictable increase in the Ce/Yb ratio (from 10 to 17; Table 4).

The bulk of the REE enrichment in the Strange Lake pluton was associated with the emplacement of the much more evolved transsolvus granite. By the time that this granite was emplaced, arfvedsonite had begun crystallising in the magma chamber. Temperature, however,

had decreased significantly as had the Ca content of the magma, thereby ensuring that arfvedsonite crystallisation, rather than depleting the magma in the REE actually enriched it in these elements. The residue of this magma segregated to form the pegmatites, which host much of the REE resource at Strange Lake. Although the early crystallisation of arfvedsonite lead to a small depletion (<10 %) in the concentration of the HREE (black dashed line in Fig. 10), the principal role of this crystallisation was to increase the overall REE content of the melt by removing Fe, Si and Na (red line in Fig. 10). This, however, was offset by the accumulation of the REE-fluoride melt that removed the LREE and to certain extent the MREE from the silicate melt. This resulted in a modest increase in the total REE content from 4622 ppm in the transsolvus granite to 5111 ppm in the pegmatite and a decrease in the Ce/Yb ratio from 12 to 6, respectively (Table 4). In summary, the delay of the crystallisation of arfvedsonite until a relatively late stage in the evolution of the magma and the relatively low temperature and Ca content created the necessary conditions for a fertile pluton at Strange Lake.

Acknowledgments

The research was funded by a NSERC Discovery Grant. Karin Siegel provided valuable advice on the arfvedsonite chemistry and access to her data. Charlie Beard helped with advice on the mechanics of fitting mineral-melt partitioning coefficient data to the lattice strain model.

Captions

Figure 1. A geological map of the Strange Lake pluton showing the distribution of the granites, pegmatites, fluorite-hematite breccia and the locations of the samples on which this study was based (modified after Vasyukova and Williams-Jones, 2014).

Figure 2. Photographs of hand specimens of pegmatite (a), transsolvus granite (c), hypersolvus granite (e) and photomicrographs showing melt inclusions in pegmatite (b), and the mineralogy of transsolvus granite (d) and hypersolvus granite (f).

Figure 3. Chondrite-normalised REE profiles for (a) arfvedsonite in the different granitic facies, (b) the bulk rocks before correction and (c) the bulk rocks after correction. The data for chondrite were taken from Mcdonough and Sun (1995).

Figure 4. (a) A diagram showing the distribution of the arfvedsonite-melt REE partition coefficients for the M2 and M4 sites of the different granitic facies at Strange Lake as a function of ionic radius. Also shown are the ideal radii (vertical dashed

lines) for these sites in a K-richterite reported by Bottazzi et al. (1999). (b) The diagram shown in (a) to which the distribution of partition coefficients modelled separately for M2 and M4 sites using lattice strain theory have been added (dashed curves). (c) the diagram shown in (b) after correction for the partitioning of REE between the M2 and M4 sites. Also shown (yellow diamonds) are the ideal radii for the two sites. For further detail refer to text.

Figure 5. Binary plots of the concentrations of (a) Ca versus Al (apfu) and (b) LREE versus Al (apfu) in arfvedsonite from the different granitic units.

Figure 6. Binary plots of the lattice strain parameters (r_0, E_M and D_0) versus the CaO content (wt. %) of the M4 site (a-c) and temperature (K) for the M2 site (d-f).

Figure 7. Binary plots of the measured REE concentrations of the different granitic units versus the modelled concentrations (ppm). For information on the absolute concentrations of the REE and the differences between the measured and modelled concentrations readers are referred to Tables 4 and 7, respectively.

Figure 8. A diagram showing the distribution of the arfvedsonite-melt REE partition coefficients for the M2 and M4 sites of the Amis granitic pegmatite as a function of ionic radius (orange diamonds). Also shown is the distribution of these partition coefficients determined using the model developed in this study (dashed curve).

Figure 9. (a) Modelled melt/arfvedsonite REE partition coefficients for a selection of temperatures for arfvedsonite with 0.47 wt. % CaO. The temperature independence of the partition coefficients for La to Eu reflects the fact that incorporation of the REE in the M4 site is insensitive to temperature. In contrast, incorporation of the REE in the M2 site (Gd to Lu) is strongly dependent on temperature. (b) Modelled melt/arfvedsonite REE partition coefficients for the various granite facies and pegmatite in the Strange Lake granite.

Figure 10. A chondrite-normalised diagram showing (1) the distribution of the REE in the transsolvus granite magma before crystallisation of arfvedsonite (blue), (2) the enrichment of the REE after removing 20 wt. % arfvedsonite without considering the REE content of the arfvedsonite (red) and (3) the depletion in the HREE resulting from consideration of the latter (black dashed).

References

Blundy, J., Wood, B., 2003. Partitioning of trace elements between crystals and melts. Earth and Planetary Science Letters, 210(3-4): 383-397.

Bottazzi, P., Tiepolo, M., Vannucci, R., Zanetti, A., Brumm, R., Foley, S.F., Oberti, R., 1999. Distinct site preferences for heavy and light REE in amphibole and the prediction of D-Amph/L(REE). Contributions to Mineralogy and Petrology, 137(1-2): 36-45.

Gysi, A.P., Williams-Jones, A.E., 2013. Hydrothermal mobilization of pegmatite-hosted REE and Zr at Strange Lake, Canada: A reaction path model. Geochimica et Cosmochimica Acta, 122: 324-352.

Gysi, A.P., Williams-Jones, A.E., Collins, P., 2016. Lithogeochemical vectors for hydrothermal processes in the Strange Lake peralkaline granitic REE-Zr-Nb deposit. Economic Geology, 111: 1241-1276.

Mcdonough, W.F., Sun, S.S., 1995. The Composition of the Earth. Chemical Geology, 120(3-4): 223-253.

Miller, R.R., Heaman, L.M., Birkett, T.C., 1997. U-Pb zircon age of the Strange Lake peralkaline complex: Implications for Mesoproterozoic peralkaline magmatism in north-central Labrador. Precambrian Research, 81(1-2): 67-82.

Olin, P.H., Wolff, J.A., 2010. Rare earth and high field strength element partitioning between iron-rich clinopyroxenes and felsic liquids. Contributions to Mineralogy and Petrology, 160(5): 761-775.

Salvi, S., Williams-Jones, A.E., 1995. Zirconosilicate Phase-Relations in the Strange Lake (Lac-Brisson) Pluton, Quebec-Labrador, Canada. American Mineralogist, 80(9-10): 1031-1040.

Salvi, S., Williams-Jones, A.E., 1996. The role of hydrothermal processes in concentrating high-field strength elements in the Strange Lake peralkaline complex, northeastern Canada. Geochimica et Cosmochimica Acta, 60(11): 1917-1932.

Schmitt, A.K., Trumbull, R.B., Dulski, P., Emmermann, R., 2002. Zr-Nb-REE mineralization in peralkaline granites from the Amis Complex, Brandberg (Namibia): Evidence for magmatic pre-enrichment from melt inclusions. Economic Geology and the Bulletin of the Society of Economic Geologists, 97(2): 399-413.

Siegel, K., 2018. The origin and magmatic evolution of the REE-rich strange lake A-type peralkaline granite, northern Québec-Labrador, Canada, McGill University Libraries, [Montreal], 298 pp.

Siegel, K., Vasyukova, O.V., Williams-Jones, A.E., 2018. Magmatic evolution and controls on rare metal-enrichment of the Strange Lake A-type peralkaline granitic pluton, Québec-Labrador. Lithos, 308-309: 34-52.

Siegel, K., Williams-Jones, A.E., van Hinsberg, V.J., 2017. The amphiboles of the REE-rich A-type peralkaline Strange Lake pluton – fingerprints of magma evolution. Lithos, 288: 156-174.

Vasyukova, O., Williams-Jones, A.E., 2016. The evolution of immiscible silicate and fluoride melts: Implications for REE ore-genesis. Geochimica et Cosmochimica Acta, 172: 205-224.

Vasyukova, O.V., Williams-Jones, A.E., 2014. Fluoride–silicate melt immiscibility and its role in REE ore formation: Evidence from the Strange Lake rare metal deposit, Quebec-Labrador, Canada. Geochimica et Cosmochimica Acta, 139: 110-130.

Vasyukova, O.V., Williams-Jones, A.E., 2018. Direct measurement of metal concentrations in fluid inclusions, a tale of hydrothermal alteration and REE ore formation from Strange Lake, Canada. Chemical Geology, 483: 385-396.

Vasyukova, O.V., Williams-Jones, A.E., Blamey, N.J.F., 2016. Fluid evolution in the Strange Lake granitic pluton, Canada: Implications for HFSE mobilisation. Chemical Geology, 444: 83-100.

Wood, B.J., Blundy, J.D., 1997. A predictive model for rare earth element partitioning between clinopyroxene and anhydrous silicate melt. Contributions to Mineralogy and Petrology, 129(2-3): 166-181.

Wood, B.J., Blundy, J.D., 2014. 3.11 - Trace Element Partitioning: The Influences of Ionic Radius, Cation Charge, Pressure, and Temperature. In: Holland, H.D., Turekian, K.K. (Eds.), Treatise on Geochemistry (Second Edition). Elsevier, Oxford, pp. 421-448.

Figure

Vasyukova, O.V., Williams-Jones, A.E., 2019. Tracing the evolution of a fertile REE granite by modelling amphibole-melt partitioning, the Strange Lake story. Chemical Geology, 514: 79-89.

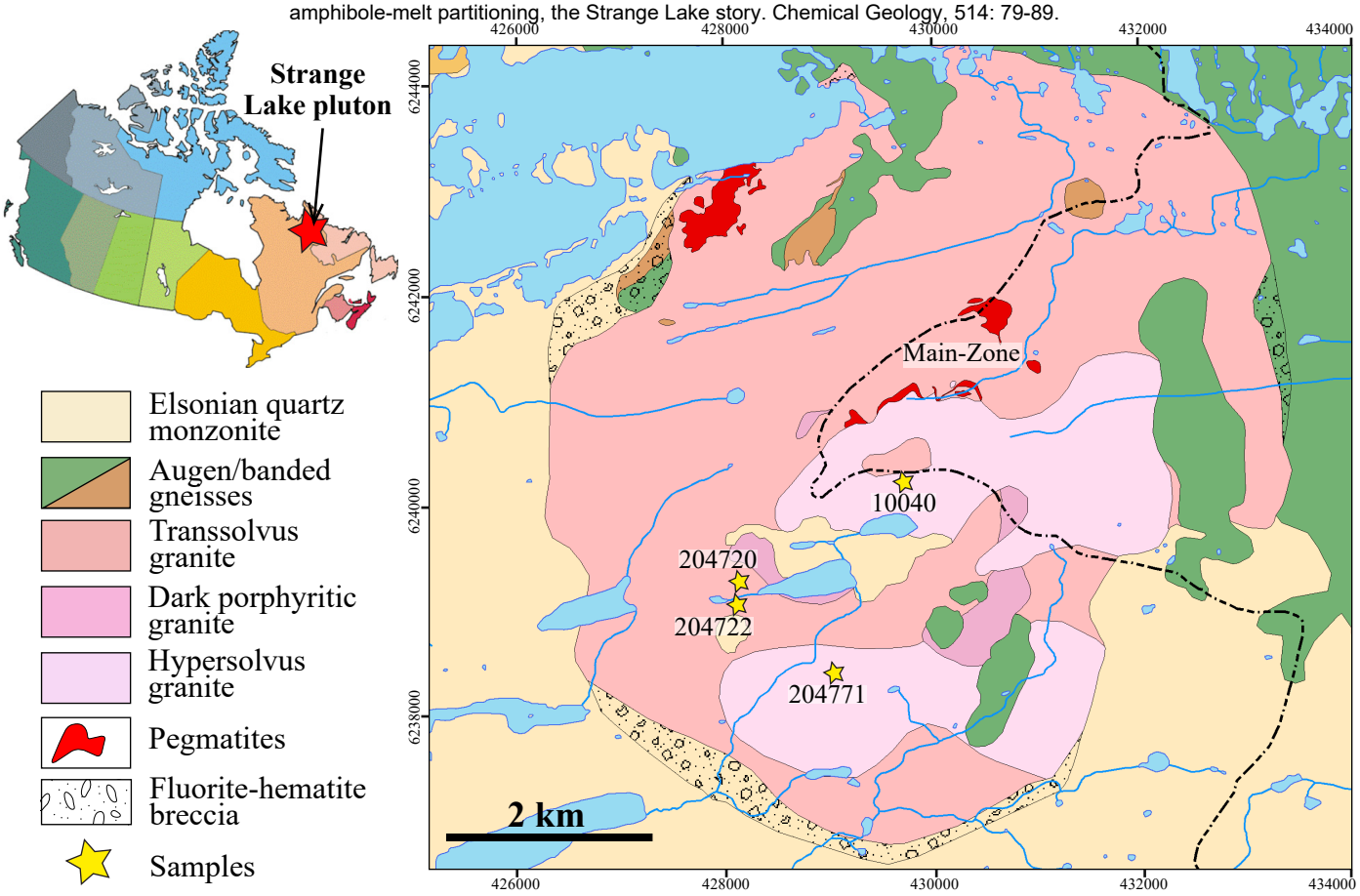

Figure 1 A geological map of the Strange Lake pluton showing the distribution of the granites, pegmatites, fluorite-hematite breccia and the locations of the samples on which this study was based (modified after Vasyukova and Williams-Jones, 2014).

Vasyukova, O.V., Williams-Jones, A.E., 2019. Tracing the evolution of a fertile REE granite by modelling amphibole-melt partitioning, the Strange Lake story. Chemical Geology, 514: 79-89.

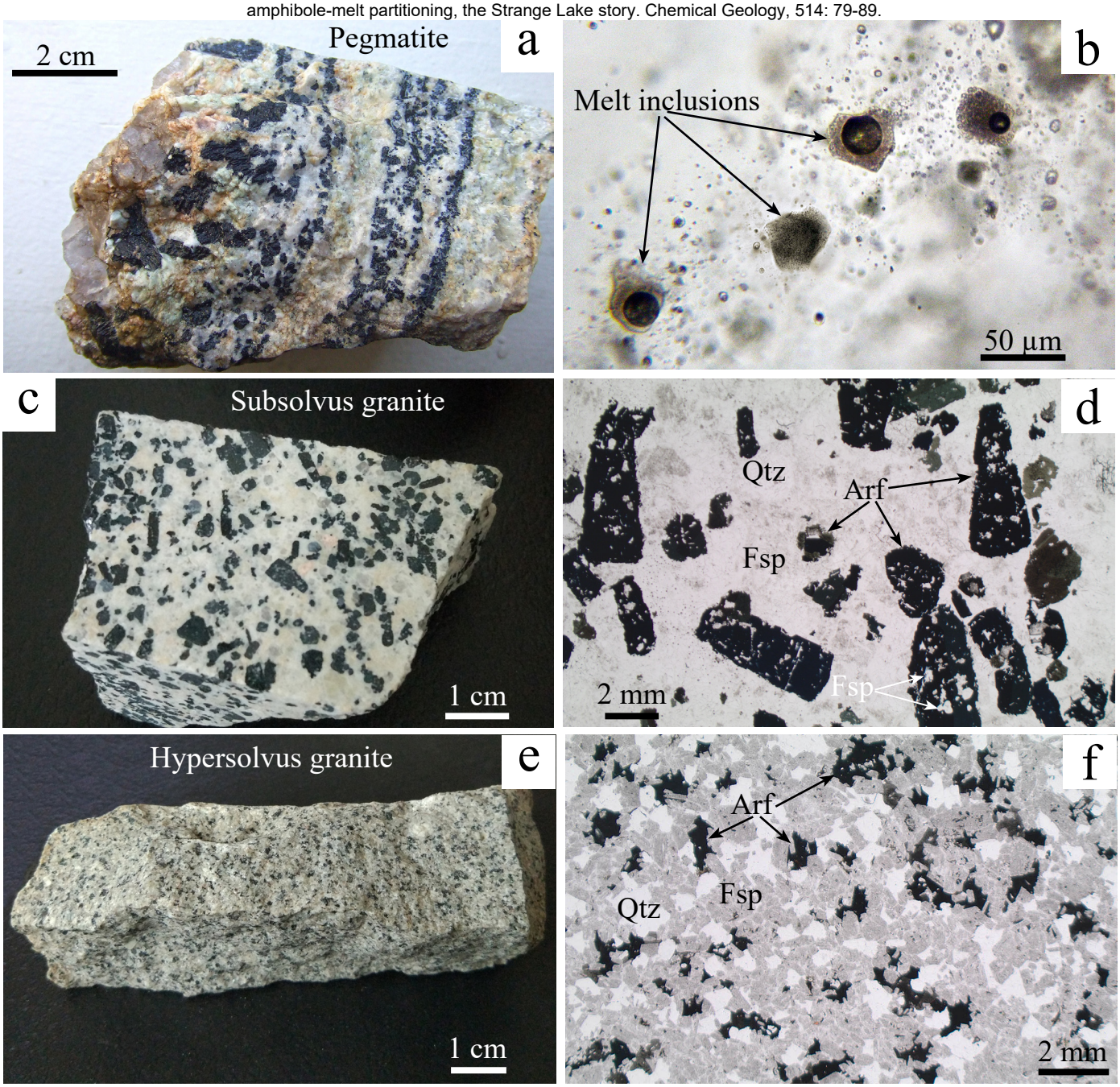

Figure 2 Photographs of hand specimens of pegmatite (a), transsolvus granite (c), hypersolvus granite (e) and photomicrographs showing melt inclusions in pegmatite (b), and the mineralogy of transsolvus granite (d) and hypersolvus granite (f).

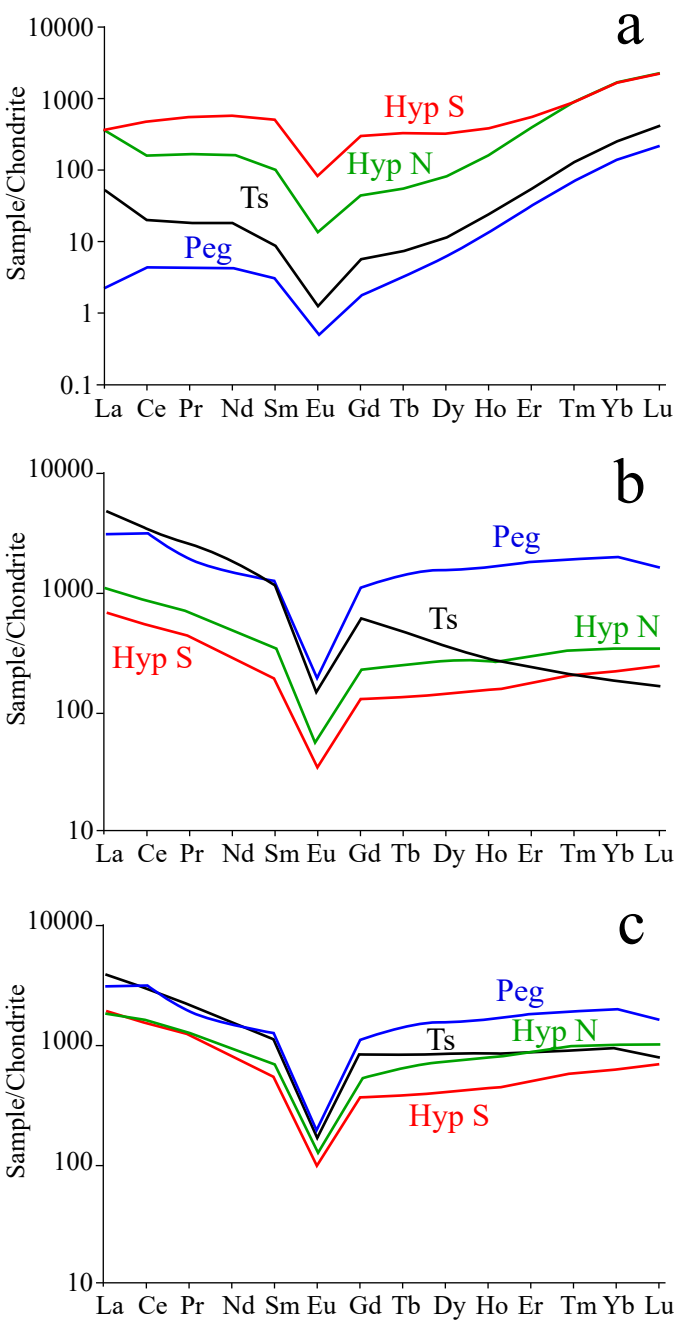

Figure 3 Chondrite-normalised REE profiles for (a) arfvedsonite in the different granitic facies, (b) the bulk rocks before correction and (c) the bulk rocks after correction. The data for chondrite were taken from Mcdonough and Sun (1995).

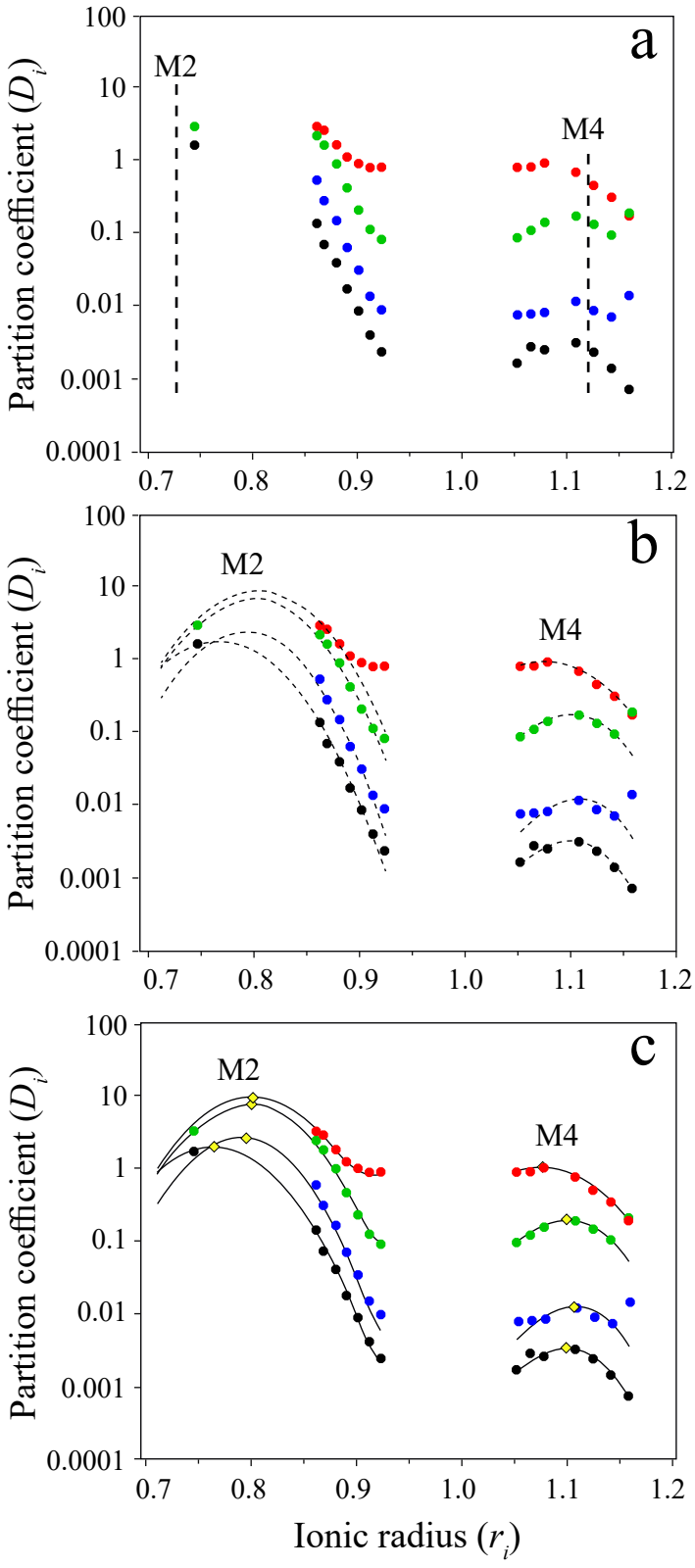

Figure 4 (a) A diagram showing the distribution of the arfvedsonite-melt REE partition coefficients for the M2 and M4 sites of the different granitic facies at Strange Lake as a function of ionic radius. Also shown are the ideal radii (vertical dashed lines) for these sites in a K-richterite reported by Bottazzi et al. (1999). (b) The diagram shown in (a) to which the distribution of partition coefficients modelled separately for M2 and M4 sites using lattice strain theory have been added (dashed curves). (c) the diagram shown in (b) after correction for the partitioning of REE between the M2 and M4 sites. Also shown (yellow diamonds) are the ideal radii for the two sites. For further detail refer to text.

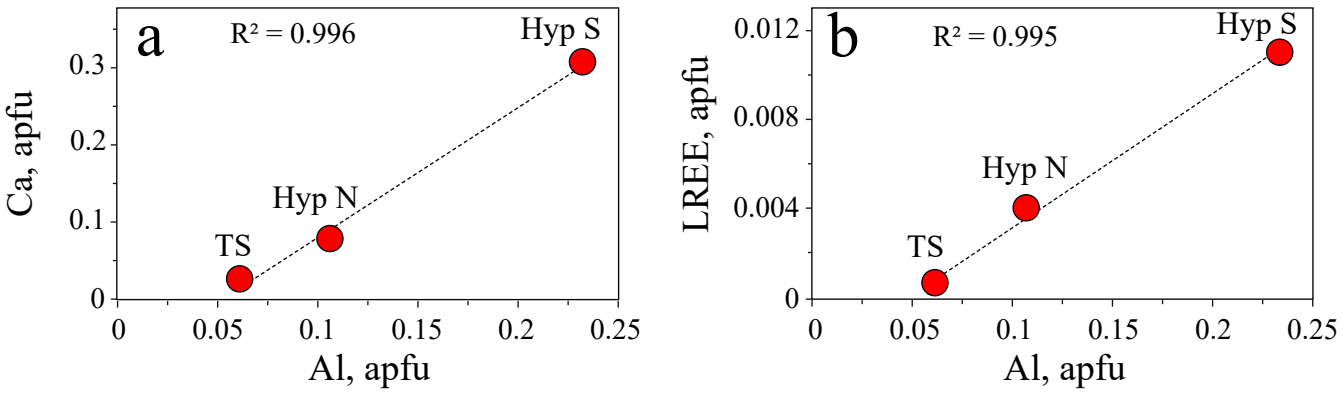

Figure 5 Binary plots of the concentrations of (a) Ca versus Al (apfu) and (b) LREE versus Al (apfu) in arfvedsonite from the different granitic units.

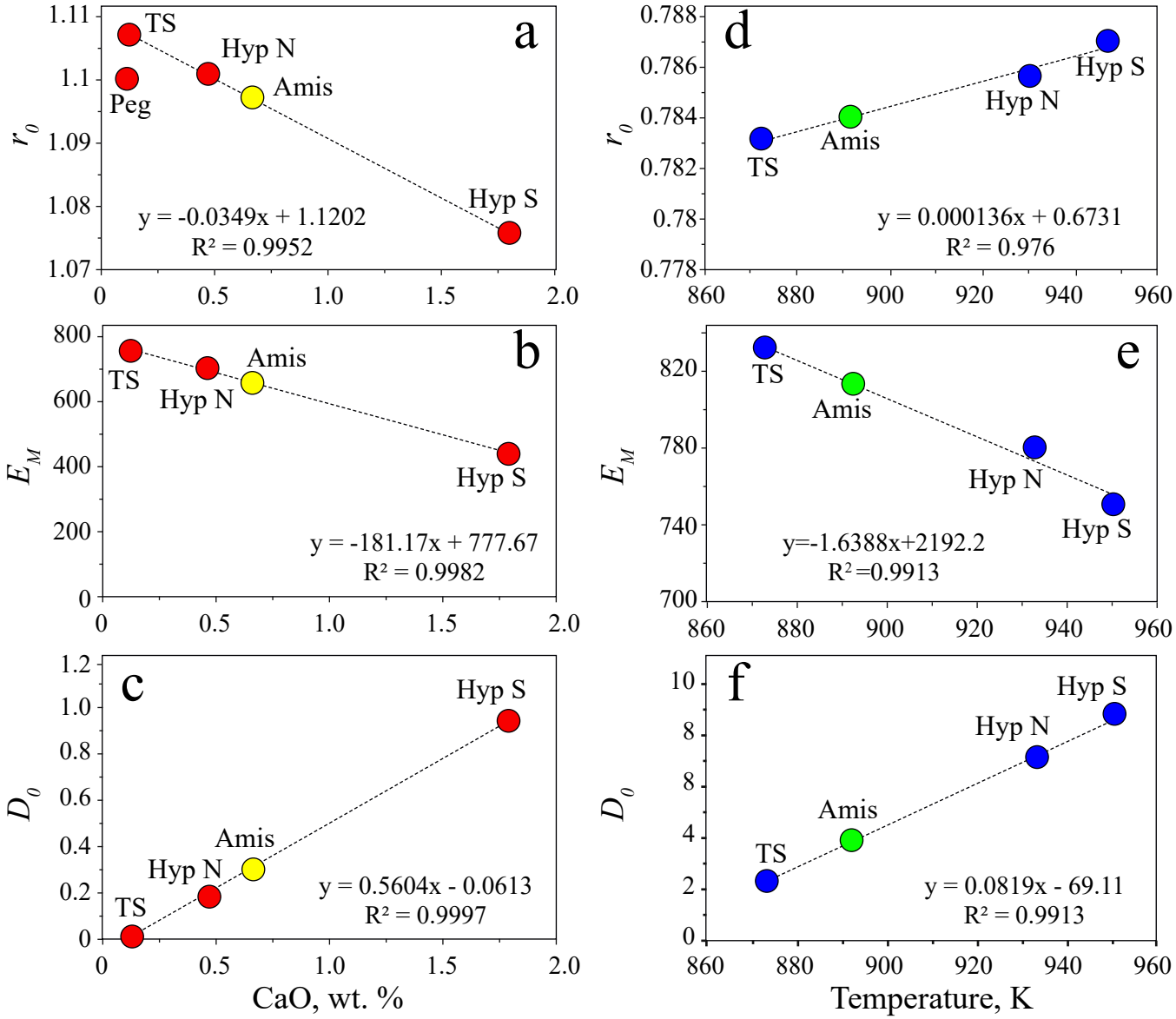

Figure 6 Binary plots of the lattice strain parameters (r0, EM and D0) versus the CaO content (wt. %) of the M4 site (a-c) and temperature (K) for the M2 site (d-f).

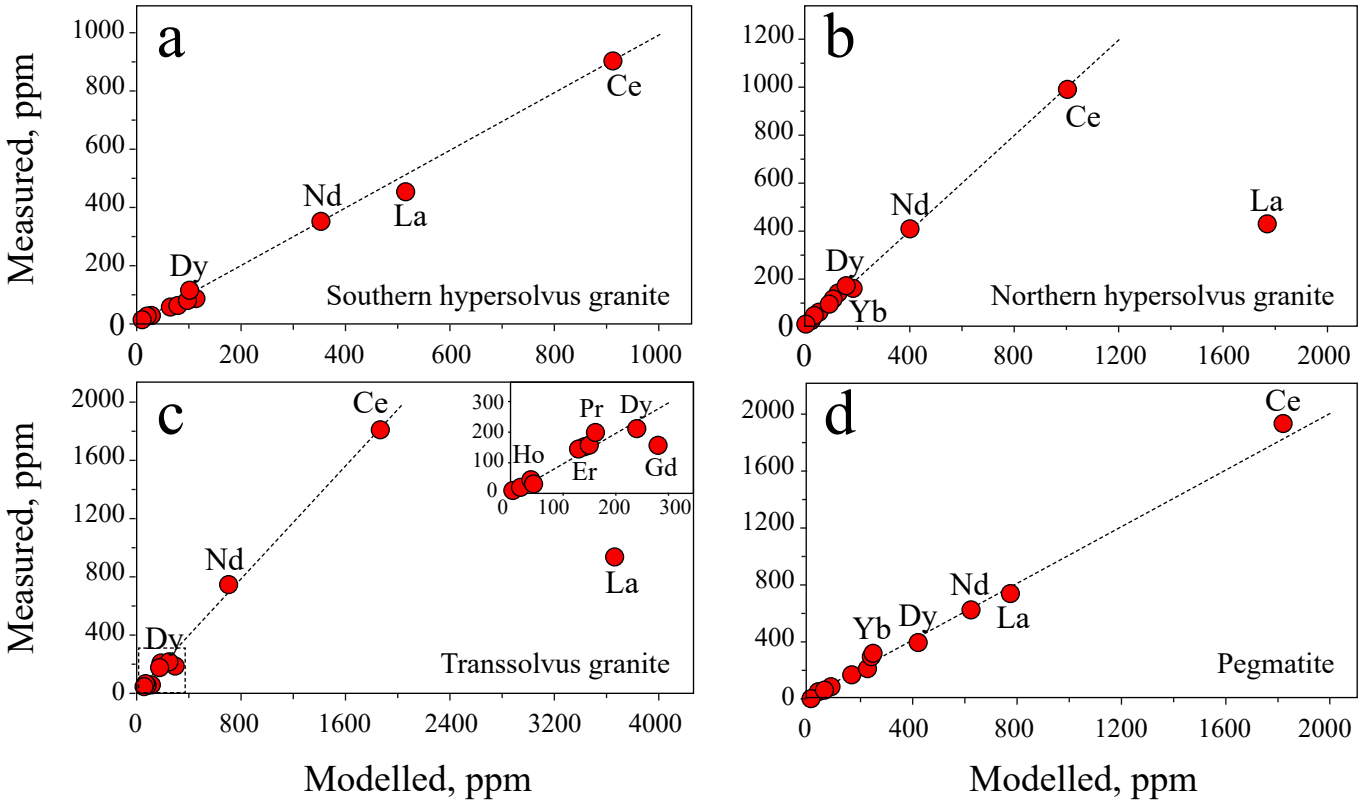

Figure 7 Binary plots of the measured REE concentrations of the different granitic units versus the modelled concentrations (ppm). For information on the absolute concentrations of the REE and the differences between the measured and modelled concentrations readers are referred to Tables 4 and 7, respectively.

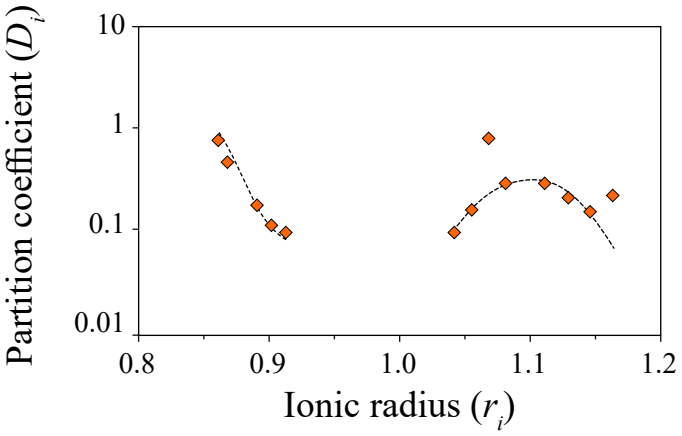

Figure 8 A diagram showing the distribution of the arfvedsonite-melt REE partition coefficients for the M2 and M4 sites of the Amis granitic pegmatite as a function of ionic radius (orange diamonds). Also shown is the distribution of these partition coefficients determined using the model developed in this study (dashed curve).

Vasyukova, O.V., Williams-Jones, A.E., 2019. Tracing the evolution of a fertile REE granite by modelling amphibole-melt partitioning, the Strange Lake story. Chemical Geology, 514: 79-89.

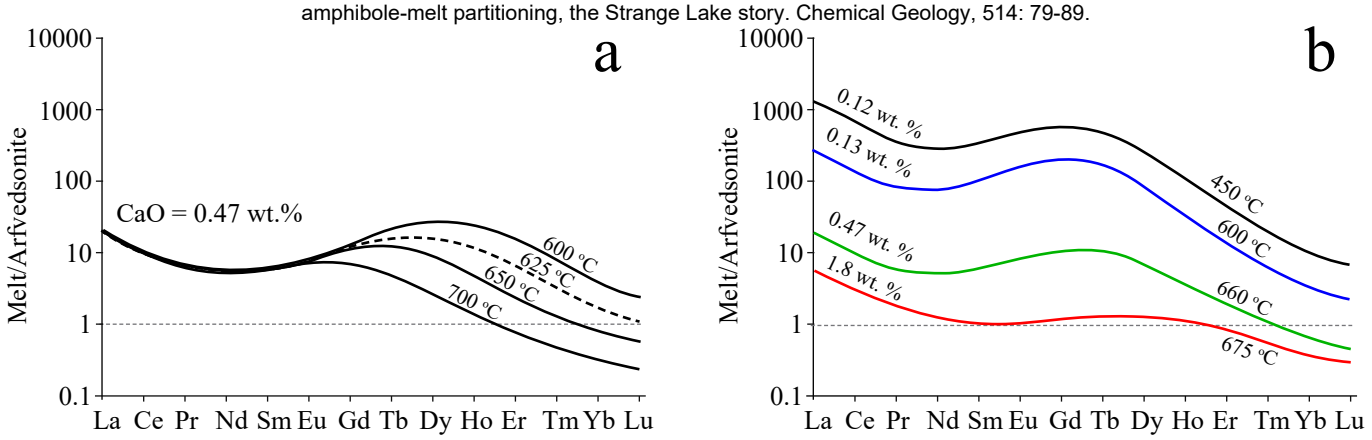

Figure 9 (a) Modelled melt/arfvedsonite REE partition coefficients for a selection of temperatures for arfvedsonite with 0.47 wt. % CaO. The temperature independence of the partition coefficients for La to Eu reflects the fact that incorporation of the REE in the M4 site is insensitive to temperature. In contrast, incorporation of the REE in the M2 site (Gd to Lu) is strongly dependent on temperature. (b) Modelled melt/ arfvedsonite REE partition coefficients for the various granite facies and pegmatite in the Strange Lake granite.

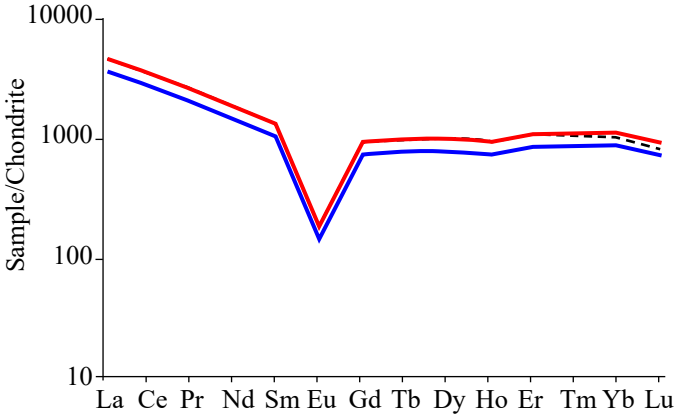

Figure 10 A chondrite-normalised diagram showing (1) the distribution of the REE in the transsolvus granite magma before crystallisation of arfvedsonite (blue), (2) the enrichment of the REE after removing 20 wt. % arfvedsonite without considering the REE content of the arfvedsonite (red) and (3) the depletion in the HREE resulting from consideration of the latter (black dashed).

Vasyukova, O.V., Williams-Jones, A.E., 2019. Tracing the evolution of a fertile REE granite by modelling amphibole-melt partitioning, the Strange Lake story. Chemical Geology, 514: 79-89.

Tables

Table 1 Mineral formulae and abbreviations.

Mineral	Ideal formula	Mineral abbreviations used in Figures
Aegirine	$NaFeSi_2O_6$	Aeg
Albite	$NaAlSi_3O_8$	Alb
Arfvedsonite	$Na_3(Fe^{2+}{}_4Fe^{3+})Si_8O_{22}(OH)_2$	Arf
Armstrongite	$CaZrSi_6O_{15}•3H_2O$	Arm
Bastnäsite-(Ce)	$(Ce,La)(CO_3)F$	Bst-(Ce)
Elpidite	$Na_2ZrSi_6O_{15}•3(H_2O)$	Elp
Ferriallanite-(Ce)	$\{CaCe\}\{Fe^{3+}AlFe^{2+}\}(Si_2O_7)(SiO_4)O(OH)$	Fe-Aln-(Ce)
Ferroceladonite	$K(Fe^{2+},Mg)(Fe^{3+},Al)(Si_4O_{10})(OH)_2$	Fe-Cel
Fluocerite-(Ce)	$(La,Ce)F_3$	FCer-(Ce)
Fluorite	CaF_2	Fl
Gadolinite	$(REE)_2Fe^{++}Be_2Si_2O_{10}$	Gad-(Ce), Gad-(Y), Gad-(Yb)
Gagarinite	$NaCaREE(F,Cl)_6$	Gag-(Ce)
Gerenite-(Y)	$(Ca,Na)_2(REE)_3Si_6O_{18}•2(H_2O)$	Ger-(Y)
Gittinsite	$CaZrSi_2O_7$	Git
Hematite	Fe_2O_3	Hm
Nahcolite	$NaHCO_3$	Nah
Narsarsukite	$Na_2(Ti_xFe^{+++}{}_{1-x})Si_4(O,F)_{11}$	Nar
Magnetite	$Fe^{2+}Fe^{3+}{}_2O_4$	Mt
Microcline	$KAlSi_3O_8$	Mcl
Perthite	$(Na,K)AlSi_3O_8$	Per
Pyrochlore	$(Na,Ca,REE)_2Nb_2O_6(OH,F)$	Pyr
Quartz	SiO_2	Qtz
Vlasovite	$Na_2ZrSi_4O_{11}$	Vls
Zircon	$ZrSiO_4$	Zrc

Table 2 Major and rare earth element composition of arfvedsonite.

Sample #	Southern hypersolvus 204771 Arfvedsonite	Northern hypersolvus 10040 Fluoro-arfvedsonite	Transsolvus 204720 Ferro-ferri-fluoro-arfvedsonite	Pegmatite 204722 Fluoro-arfvedsonite
SiO_2	48.17	50.35	51.11	51.75
TiO_2	1.00	1.21	0.77	0.34
Al_2O_3	1.26	0.59	0.35	0.29
FeO	34.09	32.36	32.54	32.46
MnO	0.70	0.83	0.56	0.65
MgO	0.30	0.23	0.07	0.11
ZnO	0.90	0.47	0.28	0.36
ZrO_2	0.09	0.14	0.13	0.09
Nb_2O_5	0.07	0.04	0.02	0.02
Na_2O	8.22	9.27	9.79	9.59
K_2O	1.08	1.58	1.65	2.04
CaO	1.80	0.47	0.12	0.11
F	1.65	2.07	2.79	2.36
Cl	0.03	0.01	0.00	0.00
Li_2O	0.50	0.62	1.23	0.72
Total	99.15	99.34	100.21	99.85
ppm				
La	87	86	13	1
Ce	291	97	13	3
Pr	52	16	2	0.4
Nd	259	74	9	2
Sm	74	15	1	0.5
Eu	5	1	0.1	0.03
Gd	60	9	1	0.4
Tb	12	2	0	0.1
Dy	80	21	3	2
Ho	21	9	1	1
Er	89	62	9	5
Tm	23	22	3	2
Yb	251	271	42	23
Lu	50	55	10	5

Table 3 Major and rare earth element composition of the different granitic units

	Southern hypersolvus granite	Northern hypersolvus granite	Transsolvus granite	Pegmatite (MI*)	Southern hypersolvus pegmatite**
Sample #	204771	10040	204720	204722	10218
Wt. %					
SiO_2	70.42	71.16	69.73	60.68	70.78
Al_2O_3	11.58	11.97	9.79	5.38	10.6
Fe_2O_3	6.08	4.82	7.22	5.83	7.47
MnO	0.10	0.10	0.12	0.20	0.11
MgO	0.04	0.05	0.02	0.002	bdl
CaO	0.55	0.61	0.32	0.11	0.36
Na_2O	4.89	5.00	4.81	9.02	5.17
K_2O	4.65	4.74	4.99	3.39	4.44
TiO_2	0.31	0.27	0.18	0.47	0.18
Nb_2O_5	0.02	0.05	0.03	0.44	0.03
P_2O_5	0.03	0.02	0.02	0.05	bdl
F	0.45	0.41	0.71	2.50	0.36
Total	99.38	98.80	97.22	89.59	99.5
ppm					
La	168	252	1140	742	203
Ce	330	540	2030	1937	466
Pr	40	62	240	168	55
Nd	131	221	880	631	204
Sm	28	49	159	181	50
Eu	2	3	8	11	3
Gd	26	45	122	220	42
Tb	5	9	17	48	7
Dy	35	63	83	389	43
Ho	8	14	15	85	8
Er	28	48	39	292	25
Tm	5	8	5	45	4
Yb	34	53	29	322	28
Lu	6	8	4	40	4

* - MI refers to melt inclusions.

** - The data for the southern hypersolvus granite pegmatite are from Siegel (2018) and were not used in determining arfvedsonite-melt REE partition coefficients.

Bdl – below the detection limit

Table 4 Corrected REE composition of the magmas.

	Southern hypersolvus	Northern hypersolvus	Transsolvus	Pegmatite (MI*)	Southern hypersolvus pegmatite
Sample #	204771	10040	204720	204722	10218
La	458	430	928	742	495
Ce	899	980	1829	1937	1137
Pr	109	114	196	168	134
Nd	357	409	736	631	498
Sm	76	100	158	181	122
Eu	5	7	9	11	7
Gd	71	99	153	220	102
Tb	14	23	29	48	17
Dy	95	173	206	389	105
Ho	22	40	44	85	20
Er	76	140	143	292	61
Tm	14	24	22	45	10
Yb	93	158	150	322	68
Lu	16	24	19	40	10
TREE	2305	2721	4622	5111	2786
Ce/Yb	10	6	12	6	17

* - MI refers to melt inclusions.

Table 5 Arfvedsonite-melt REE partition coefficients for the different granites.

	Southern hypersolvus	Northern hypersolvus	Transsolvus	Pegmatite (MI*)
Sample #	204771	10040	204720	204722
La	1.9E-01	2.0E-01	1.4E-02	7.2E-04
Ce	3.2E-01	9.9E-02	7.1E-03	1.4E-03
Pr	4.8E-01	1.4E-01	8.8E-03	2.3E-03
Nd	7.2E-01	1.8E-01	1.2E-02	3.1E-03
Sm	9.6E-01	1.5E-01	8.2E-03	2.5E-03
Eu	8.5E-01	1.1E-01	7.8E-03	2.8E-03
Gd	8.5E-01	9.1E-02	7.9E-03	1.6E-03
Tb	8.5E-01	8.7E-02	9.4E-03	2.4E-03
Dy	8.4E-01	1.2E-01	1.4E-02	4.0E-03
Ho	9.4E-01	2.2E-01	3.1E-02	8.6E-03
Er	1.2E+00	4.4E-01	6.4E-02	1.7E-02
Tm	1.7E+00	9.4E-01	1.5E-01	3.9E-02
Yb	2.7E+00	1.7E+00	2.8E-01	7.0E-02
Lu	3.0E+00	2.3E+00	5.4E-01	1.4E-01

* - MI refers to melt inclusions.

Table 6 Modelled values for D_0, E_M and r_0 of the M4 and M2 sites.

	Southern hypersolvus	Northern hypersolvus	Transsolvus	Pegmatite (MI*)
Sample #	204771	10040	204720	204722
T, K	950	933	873	720
CaO, wt. %	1.8	0.47	0.12	0.11
M4 site				
D_0	0.95	0.19	0.013	0.003
E_M	450	700	750	600
r_0	1.076	1.101	1.107	1.1
M2 site				
D_0	9	7	2.5	1.8
E_M	750	780	830	540
r_0	0.803	0.799	0.792	0.766

* - MI refers to melt inclusions.

Table 7 The relative differences between the measured and modelled REE contents of the magmas (in %)*.

	Southern hypersolvus	Northern hypersolvus	Transsolvus	Pegmatite (MI**)
Sample #	204771	10040	204720	204722
La	-12	-310	-291	-3.0
Ce	-0.9	-3.2	-0.7	6.8
Pr	9.0	7.7	17.8	5.8
Nd	1.3	2.3	7.0	1.9
Sm	-1.3	5.9	8.8	9.5
Eu	9.9	8.1	-23	-28
Gd	2.1	1.2	-80	0.0
Tb	-6.2	3.4	-68	-20
Dy	-9.7	6.3	-14	-6.8
Ho	-0.5	16	4.2	4.0
Er	-0.4	6.6	9.4	18
Tm	-2.3	-12	-3.6	8.6
Yb	-2.4	-13	7.1	24
Lu	9.6	-12	-20	2.6

* - The absolute REE contents are reported in Table 3.
** - MI refers to melt inclusions.

Vasyukova, O.V., Williams-Jones, A.E., 2019. Tracing the evolution of a fertile REE granite by modelling amphibole-melt partitioning, the Strange Lake story. Chemical Geology, 514: 79-89.

Table 8 Modelled lattice strain parameters for the Amis granitic pegmatite.

	Amis sample
T, K	893
CaO, wt. %	0.67
M4 site	
D_0	0.31
E_M	656
r_0	1.097
M2 site	
D_0	4.03
E_M	812
r_0	0.795

Table 9 Measured and modelling REE contents of the Amis granitic pegmatite magma.

	MI* (ppm)	Fluoro-arfvedsonite (ppm)	Di, modelled	Modelled (ppm)	% difference**
La	152	35	0.063	552	-235
Ce	419	64	0.143	449	-9
Pr	56	11	0.230	50	10
Nd	224	63	0.297	212	5
Sm	75	21	0.279	77	-3
Eu	1	1	0.223	3	-238
Gd	123	19	0.159	122	0
Tb	31	3	0.101	29	12
Dy	177	17	0.129	129	-13
Ho	32	4	0.171	21	-7
Er	84	15	0.260	57	-1
Tm	-	4	0.408	9	0
Yb	106	48	0.714	67	27
Lu	15	11	0.971	11	15

* - MI refers to melt inclusions.

** - The proportional difference between the modelled and measured concentration.